# On the Solution of a Class of Large Body Problems with Partial Circular Symmetry (Multiple Asymmetries) by Using a Hybrid-Dimensional Finite-Difference Time-Domain (FDTD) Method

Dean Arakaki, *Member, IEEE*, Wenhua Yu, *Senior Member, IEEE*, and Raj Mittra, *Life Fellow, IEEE*

***Abstract*—This paper presents an efficient method to solve a large body scattering problem, *viz.* a paraboloid reflector antenna system, with only partial circular symmetry. The asymmetry in the system is introduced by two factors, *viz.* the microstrip feed and an inhomogeneous radome. The paper presents a novel approach, based on the equivalence and reciprocity principles and the "equivalent" aperture theory, to overcome the asymmetry problem. The technique thereby enables substantial computational efficiencies by analyzing the majority of the three-dimensional (3-D) computational domain in an effective two-dimensional (2-D) simulation, with the remainder being analyzed using a 3-D algorithm.**

***Index Terms*—Finite difference time domain (FDTD), reflector antenna, radome.**

## I. Introduction

THE purpose of this paper is to efficiently compute the radiation pattern of a large, partially, circularly symmetric antenna system. To avoid a three-dimensional (3-D) simulation of the entire structure, the paper presents two techniques that exploit the circular symmetry of the problem geometry to reduce the number of dimensions required by the simulation from three to two for a majority of the problem space. The equivalence and reciprocity principles are used in the same manner as in [2], and as described in Section II-B below to overcome the first asymmetry caused by the feed structure and to construct the radiation pattern. The second asymmetry, introduced by the inhomogeneous radome, is handled by applying the "equivalent aperture" theory to divide the problem into two-dimensional (2-D) (majority of the simulation domain) and 3-D analyzes prior to use of the aforementioned principles for the computation of the radiation pattern. The finite-difference time-domain (FDTD) [1] method is used to both construct the "equivalent aperture" (2-D FDTD) and to propagate these aperture fields in a 3-D FDTD simulation whose results are used by the reciprocity theorem to construct the pattern (see Section II-B).

The FDTD technique is a method well suited for the simulation of the electromagnetic scattering properties of complex geometries composed of inhomogeneous material [1]. The solution to the circularly symmetric portion of the problem is based on a 2.5-D FDTD algorithm, designed to handle Maxwell's equations for rotationally symmetric geometries [3]. The 2.5-D and 3-D FDTD simulation regions were truncated by a first-order Mur [4] and a six-layer perfectly matched layer (PML) [5] absorbing boundary condition, respectively. The application of this technique is illustrated by considering the example of a paraboloid reflector antenna system. The two asymmetries to the otherwise circularly symmetric structure are introduced by the microstrip array feed system comprising four patches, and the radome with a skirt (with dissimilar material properties), that encloses the reflector antenna subsystem. The latter asymmetry arises when the reflector antenna points off-boresight through the radome/skirt enclosure.

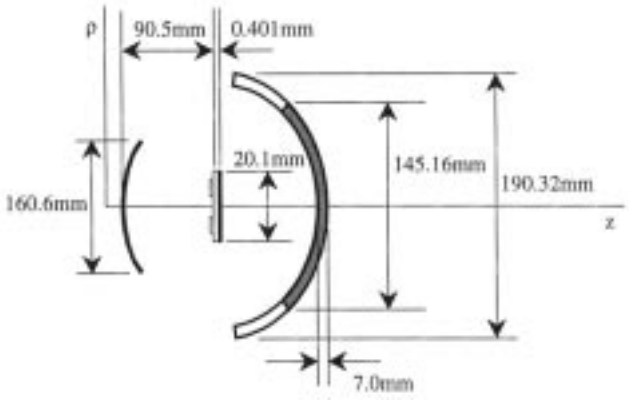


Fig. 1. Reflector antenna system.

## II. Method

### A. Problem Geometry

We consider the reflector antenna system, shown in Fig. 1, to outline the procedure. In this figure, the structures to the left, middle, and right are the main reflector (paraboloid), microstrip feed array, and the radome structure (composed of two dissimilar materials), respectively. The antenna has an aperture diameter of 160.6 mm (24.09 $\lambda$), a focal length of 90.5 mm (13.58 $\lambda$), and an operating frequency of 45 GHz. The radome has an outer diameter (including the skirt) of 190.32 mm (28.55 $\lambda$), an inner radome diameter of 145.16 mm (21.77 $\lambda$), and a thickness of 7.0 mm (1.05 $\lambda$). The inner radome and outer skirt are composed of low loss (loss tangent less than 0.001) dielectric with

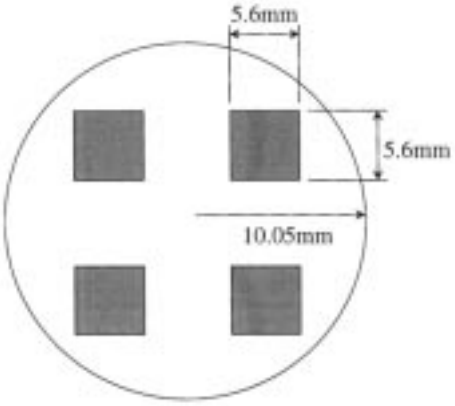


Fig. 2. Microstrip patch antenna geometry.

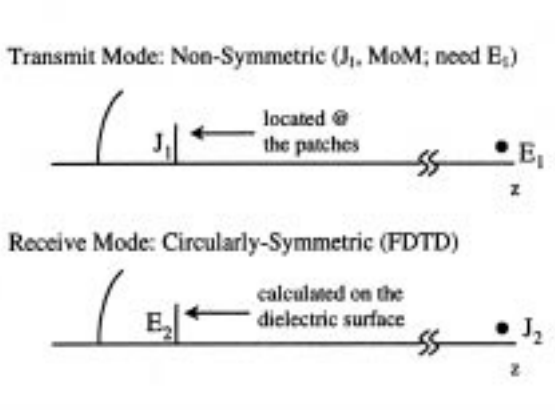


Fig. 3. Application of equivalence and reciprocity theorems to original system.

relative permittivities of 8.5 and 4.2, respectively. The feed antenna dielectric has a dielectric constant of 4.6. Fig. 2 shows the feed antenna structure as seen from the reflector.

When the reflector antenna together with its feed system points at boresight (Fig. 1), the reflector as well as the radome structures are both circularly symmetric with respect to the $z$-axis, but the feed array perturbs this symmetry. Application of both the equivalence and reciprocity theorems is used to overcome this asymmetry and reduce the 3-D problem to an effective 2-D one.

### *B. Application of the Equivalence and Reciprocity Theorems*

To reduce the number of dimensions in the analysis from three to two, we first analyze the feed structure by using a method of moments (MoM) code to determine the electric currents flowing on the surface of the four microstrip patches. By the equivalence principle, the radiating patches in the feed antenna are replaced by the computed currents. This yields a circularly symmetric geometry, but with a nonsymmetric excitation source. Instead of analyzing the system in the transmitting mode, we reverse the mode of operation and compute the fields produced on the surface of the feed dielectric by a dipole source placed where the far-zone electric field is to be determined (see Fig. 3).

Because the geometry is now circularly symmetric, a 2.5-D FDTD algorithm for bodies of revolution is employed. The reciprocity theorem, which relates the fields and currents of two systems, is applied to combine the currents obtained from the MoM code and the fields determined by the FDTD code to yield the far-zone electric field. For the system described above, the reciprocity theorem leads to the form

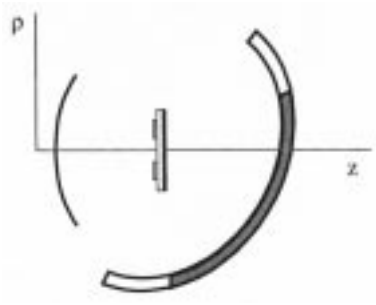


Fig. 4. Reflector antenna system, with tilted radome.

$$\int_v \vec{\boldsymbol{E}}_1 \cdot \vec{\boldsymbol{J}}_2 \, dV = \int_v \vec{\boldsymbol{E}}_2 \cdot \vec{\boldsymbol{J}}_1 \, dV, \tag{1}$$

in which $\mathbf{E_1}$ and $\mathbf{J_2}$ are the desired far-zone electric field (transmit mode) and the dipole source (receive mode) placed where $\mathbf{E_1}$ is desired, respectively. On the right-hand side, $\mathbf{E_2}$ and $\mathbf{J_1}$ are the fields produced on the surface of the circularly symmetric feed dielectric (receive mode) and the electric currents produced on the surface of the microstrip patches by the excitation sources (transmit mode), respectively. Note that the left-hand side of (1) reduces to a simple vector dot-product as $\mathbf{J_2}$ is a point source, whereas the right-hand side becomes a surface integral over the area of the four radiating patches because the electric currents $(\mathbf{J_1})$ are zero everywhere else. Also, note that $\mathbf{E_2}$ and $\mathbf{J_2}$ scale with each other; thus, $\mathbf{J_2}$ is arbitrarily set to unity. Because the right-hand side of (1) is known from the results of the MoM $(\mathbf{J_1})$ and the FDTD $(\mathbf{E_2})$ computations, the far-zone electric field $(\mathbf{E_1})$ can be determined.

### *C. Aperture Field Construction*

When the radome is tilted at an angle with respect to the axis of the reflector system, as in Fig. 4, an additional asymmetry is introduced into the geometry.

To address this problem, we first project the hybrid field pattern onto a plane perpendicular to the reflector structure ("p" in Fig. 5). In this diagram, the darker region denotes where the incident fields penetrate the higher permittivity material (radome, $\varepsilon_r = 8.5$), whereas the lighter region indicates the corresponding region illuminated by the fields that penetrate the lower permittivity material (skirt, $\varepsilon_r = 4.2$).

The fields within these regions are obtained by analyzing the "normal" configuration (Fig. 1) using a 2.5-D FDTD simulation (because the geometry has been made circularly symmetric by the equivalence principle, as described in Section II-B) with the entire radome consisting of the higher permittivity material $(\varepsilon_r = 8.5)$ first, and then the lower permittivity material $(\varepsilon_r = 4.2)$. These fields are stored in a 2-D map (for both cases) at a $z$-position just inside the main reflector (between the main reflector and radome; see Fig. 1), and then used to construct the "equivalent aperture" for the desired configuration and tilt angle. Note that the aperture fields are taken from those inter-

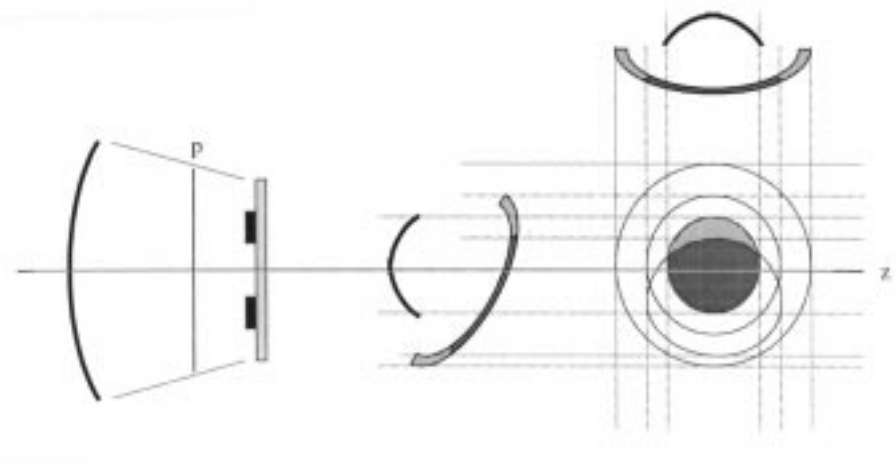


Fig. 5. Tilted radome and projected field distribution.

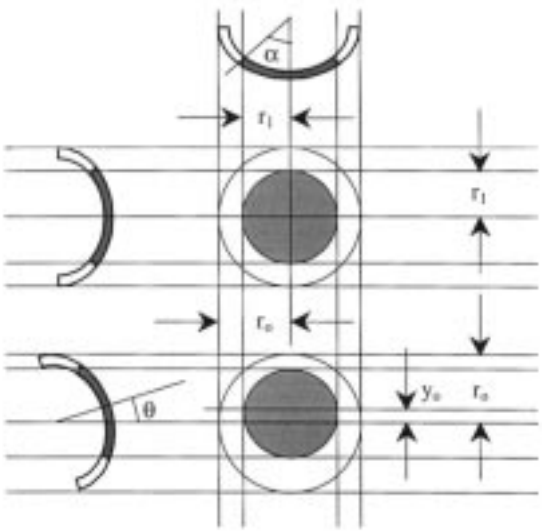


Fig. 6. Tilted radome and projected field distribution, with parameter definitions.

cepted by the main reflector and focused onto the feed, because fields not captured by the main reflector have negligible effect on those produced on the feed structure.

Because the radome is circularly symmetric about the $z$-axis, it is sufficient to analyze the system with respect to one tilt angle, chosen to be in the elevation $(yz)$ plane. A diagram of the system describing the parameters used for the aperture field construction is shown in Fig. 6.

A circular region is formed when the reflector system is aligned with the radome structure (normal incidence, top drawing), whereas an elliptical pattern results when the radome structure is tilted relative to the reflector system (bottom drawing) by an angle $\theta$.

The center of the ellipse (or circle, in the normal case), relative to the center of the pattern, is determined by

$$y_o = r_o \sin\theta \cos\alpha, \tag{2}$$

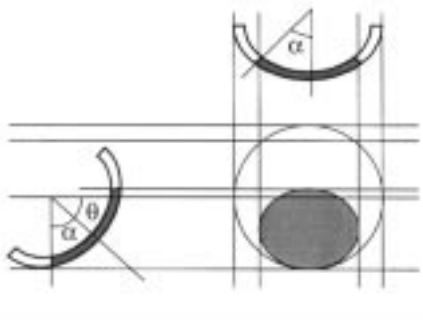


Fig. 7. Tilted radome: $\theta - \alpha = -90°$.

which is the center point between the top and bottom edges of where the radome material begins. The angle $\alpha$ is the angular displacement of the radome material, and $\theta$ is the tilt angle of the radome structure with respect to the reflector system. Because the system is tilted in the elevation plane only, the major axis of the ellipse remains fixed at a length of $r_1$ (see Fig. 6). The minor axis is calculated by the formula $b = r_1 \cos\theta$. With all of the parameters known, the equation of the ellipse can then be written as

$$\left(\frac{x}{a}\right)^2 + \left(\frac{y - y_o}{b}\right)^2 = 1, \tag{3}$$

in which $a = r_1$.

A condition that must be checked to obtain the correct aperture pattern is when $\theta - \alpha \leq -90°$ or $\theta + \alpha \geq 90°$. At these tilt angles, the bottom (top) edge of the ellipse begins to rise above (sink below) the top (bottom) edge of the radome structure. The condition of $\theta - \alpha = -90°$ is illustrated in Fig. 7.

To correct the elliptical pattern for angles beyond this special condition, the minor axis has been defined as two separate parameters, a lower and an upper length. When the condition is satisfied, the lower (upper) minor axis is defined as the difference between $r_o$ and the height of the center of the ellipse (2) for the $\theta - \alpha \leq -90°$ $(\theta + \alpha \geq 90°)$ case. The upper (lower) minor axis remains the same $(b = r_1 \cos\theta)$. To illustrate the effect of this correction, a drawing of the pattern for $\theta = -90°$ is shown in Fig. 8 in which the upper minor axis is zero.

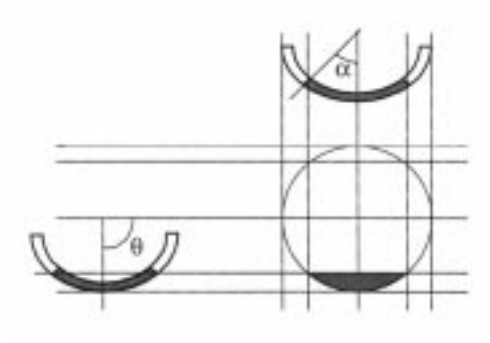


Fig. 8. Tilted radome: $\theta = -90°$.

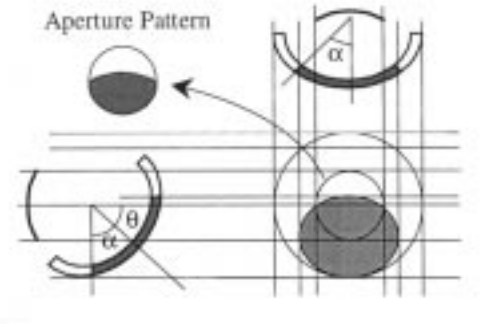


Fig. 9. Projection of distribution onto radiating aperture.

Once the distribution has been determined in the manner described above, it must be projected onto the radiating aperture of the reflector system. An example is shown in Fig. 9.

The upper left drawing in Fig. 9 shows the resulting aperture distribution projected onto the main reflector. The area of this aperture field distribution must then be adjusted (see Fig. 5) based on the distance separating the aperture and the main reflector (full-size if the aperture is located at the main reflector and zero area if located at the focal point of the main reflector). Next, this distribution is used as the input source for a 3-D FDTD simulation to propagate the fields onto the surface of the feed dielectric substrate. These fields are subsequently used to calculate the far-zone fields in accordance with the procedure described in Section II-B.

### *D. 3-D FDTD Simulation*

To compute the radiation pattern for the reflector antenna system, we must first determine the fields on the surface of the dielectric substrate, upon which the feed array resides. These fields are then used in the reciprocity approach, described in Section II-B, to calculate the far-zone fields. Because the aperture distribution, determined from the procedure described in the last section, lacks circular symmetry, a 3-D FDTD algorithm is needed to determine the fields produced on the surface of the feed dielectric. The 3-D region simulated comprises $140 \times 140 \times 40$ (784 000) cells, of which an $80 \times 80$ cell 2-D region, located at the dielectric substrate, is Fourier-transformed into the frequency domain. These resultant fields are then used in the reciprocity approach described in Section II-B to determine the far-zone radiation pattern for the entire reflector antenna system.

## III. Numerical Results

To illustrate the procedure described in the last section, we calculate the field distribution in the focal region of a paraboloidal reflector antenna. We compute the aperture fields for the radome in two steps; first for the higher permittivity material ($\varepsilon_r = 8.5$) and then for the lower one ($\varepsilon_r = 4.2$). These distributions are shown in Figs. 10 and 11, respectively. For this analysis, the tilt angle of the radome with respect to the reflector system was 30°. The elliptical pattern projected onto the receiving aperture region, and the resulting aperture pattern for this tilt angle, are displayed in Figs. 12 and 13. The fields in the upper portion of Fig. 13 correspond to those of Fig. 10 (fields through the higher permittivity material), whereas the lower portion corresponds to the fields in Fig. 11 (fields through the lower permittivity material). The regions of the combined pattern are defined in the center circle of Fig. 12, which shows the aperture intercepting the incident radiation.

As mentioned earlier, these aperture patterns were subsequently used as sources for the 3-D FDTD simulation to determine the fields on the surface of the feed dielectric. In accordance with the reciprocity procedure (1), a dot product of these fields and the surface currents on the four patches were evaluated to compute the far-zone electric field. Three different cases for the surface currents were considered, along with three different reflector system tilt angles.

The three current phasing configurations analyzed were the sum, azimuthal difference, and elevation difference patterns, which are created by controlling the relative phasing between excitation sources to the patches. The sum pattern has a peak in the normal direction (all patches fed in-phase relative to the circularly polarized transmitted wave), whereas for the azimuthal and elevation difference patterns, a null exists along the $y$- and $x$-axes, respectively (see Fig. 14).

For difference patterns, the system will be sensitive to differences across the null plane. The tilt angle analyzed was in the $yz$-plane with respect to the $z$-axis (out of Fig. 14). As a result, the azimuthal difference pattern should be largely insensitive to the tilt angle because differences in fields incident on patches 1 and 4 versus those on patches 2 and 3 (along the null) should be small.

For the elevation difference pattern, a null exists along the $x$-axis. Therefore, this pattern should be sensitive to differences in the fields incident on patches 1 versus 4 and 2 versus 3. Because the tilt angle is in the $yz$-plane, fields of varying magnitude are intercepted by these pairs of patches due to the different radome materials as the tilt angle increases. This should lead to a larger change in radiated electric field magnitude.

The system was analyzed for tilt angles of 30°, 40°, and 50°. All far-zone field magnitudes were normalized to the sum pattern magnitude at boresight (0°). Both copolarization (left-hand circular polarization) and cross polarization (right-hand circular

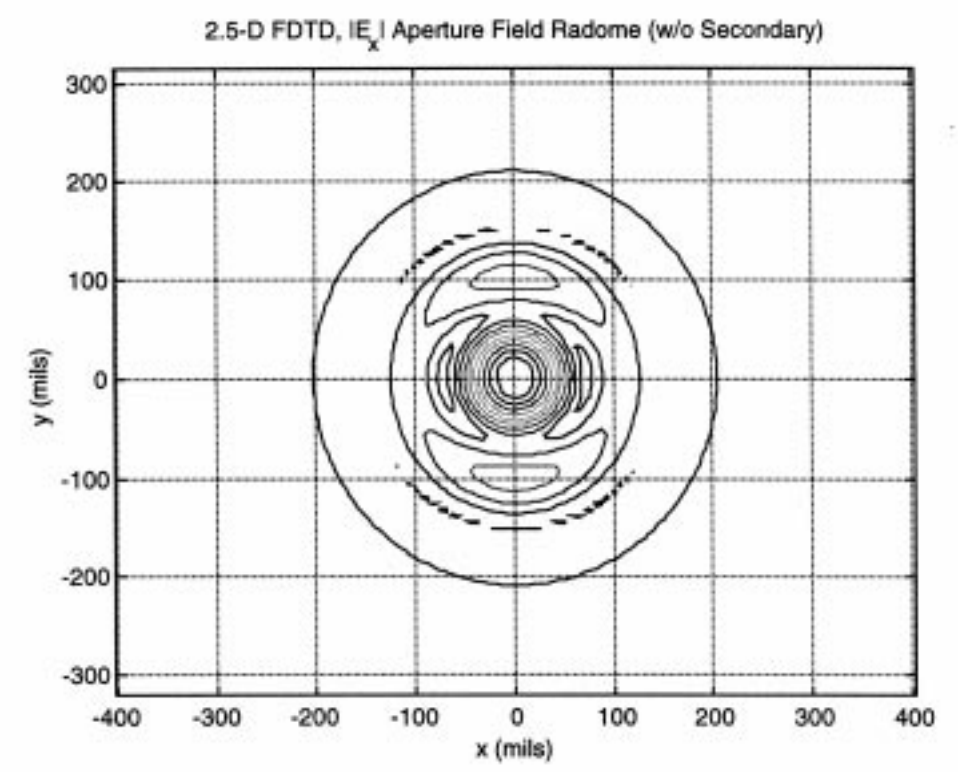


Fig. 10. Aperture field through higher permittivity material ($\varepsilon_r = 8.5$).

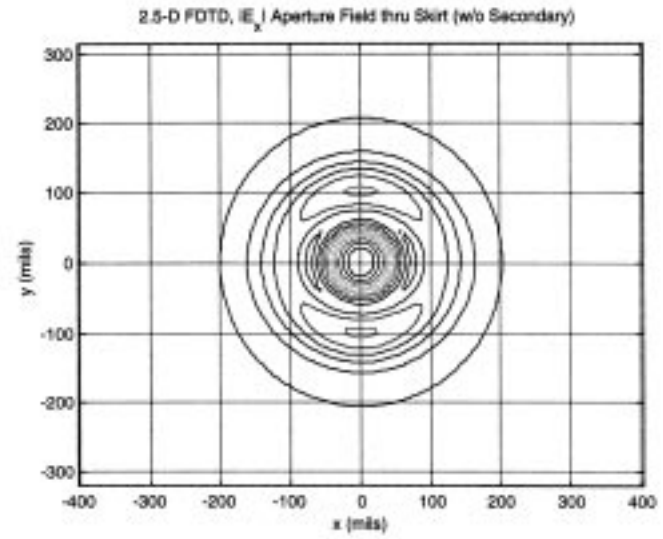


Fig. 11. Aperture field through lower permittivity material ($\varepsilon_r = 4.2$).

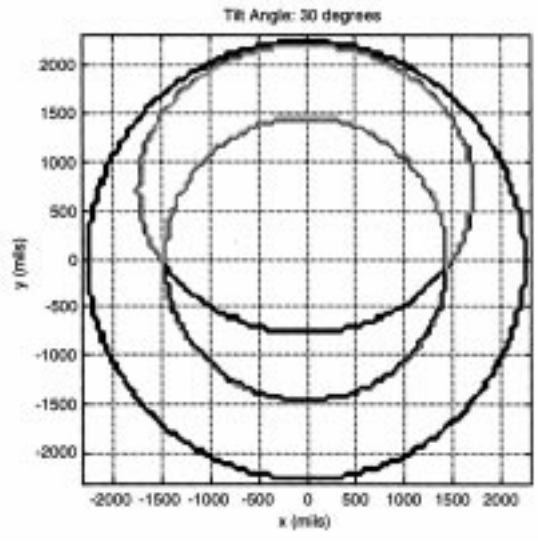


Fig. 12. Elliptical radome pattern projection onto radiating aperture.

polarization) were plotted for the three excitation phasing arrangements. The pattern for the sum pattern is shown in Fig. 15.

Due to a broad peak appearing at boresight, the radiated field magnitude was insensitive to the tilt angle, which is the expected result, as explained above. The field pattern for the azimuthal difference excitation is shown in Fig. 16.

This pattern also showed only a slight change in radiated field magnitude due to the tilt angle being along the null. The magnitude was lower than that for the sum pattern due to the null. A difference of $-3$ dB (70.7%) from the peak magnitude was noted at a tilt angle of 50°.

For the elevation difference pattern, a significant change in radiated field magnitude was noted due to the tilt angle being perpendicular to the null (see Fig. 17). This was as expected due to the relative positions of the null and tilt angle.

## IV. Conclusion

This paper has presented an efficient method for determining radiation patterns for an electrically large reflector

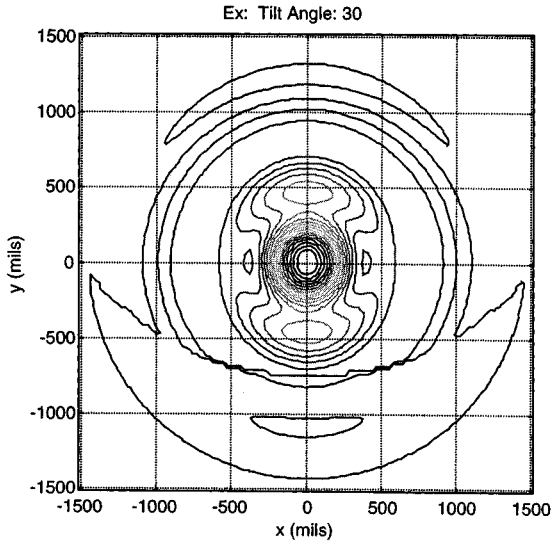


Fig. 13. Resultant aperture field pattern.

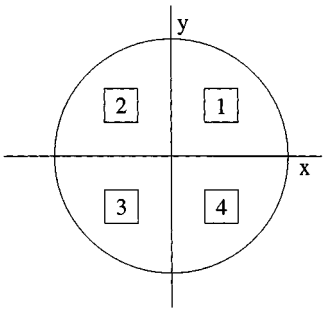


Fig. 14. Patches on feed dielectric surface.

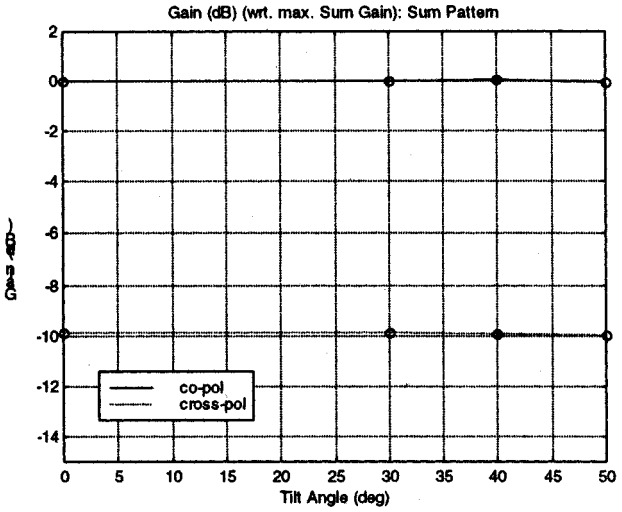


Fig. 15. Sum pattern (peak at boresight) versus $yz$-plane tilt angle.

antenna system with a microstrip patch feed and a dielectric radome/skirt combination that has only partial circular-symmetry. The paper shows how we can still take advantage of the existing symmetry of a large portion of the structure to reduce the CPU time and memory requirements significantly. The equivalence and reciprocity principles described in [6]

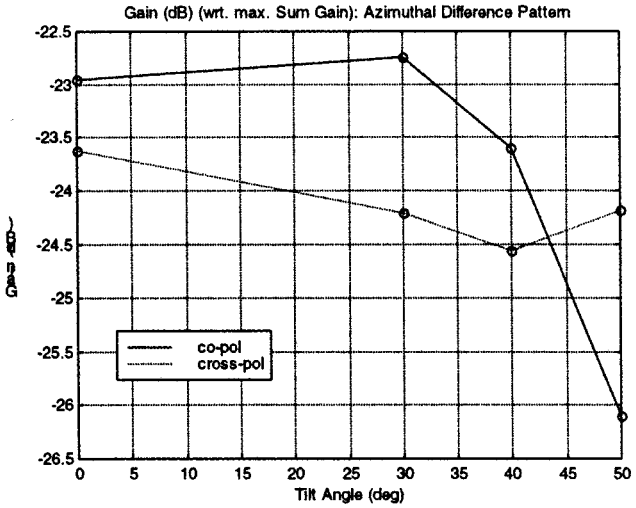


Fig. 16. Azimuthal difference pattern (null along $y$-axis) versus $yz$-plane tilt angle.

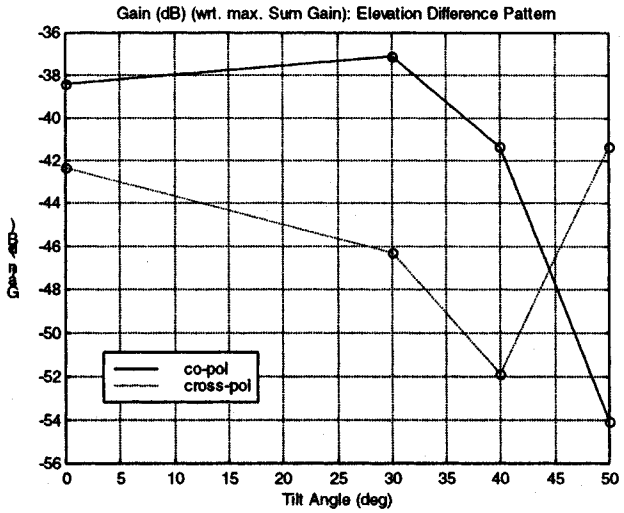


Fig. 17. Elevation difference pattern (null along $x$-axis) versus $yz$-plane tilt angle.

and Section II-B are combined with the "equivalent" aperture approach to compute the radiation pattern of the reflector antenna system. Regarding computational requirements, for the problem geometry described above, only 0.65% of the total number of cells required analysis due to the reduction from three to two dimensions for a majority (98.4%) of the computational domain. The former figure was determined from a ratio of the number of 3-D cells included in both the 2.5-D and the 3-D FDTD simulations versus the total number of 3-D cells. The latter figure was determined from the number of 2-D cells ($\rho z$-plane) simulated in the 2.5-D FDTD simulation versus the total number of 2-D cells ($\rho z$-plane). This resulted in substantial savings in terms of both memory and run-time requirements. Numerical results were presented for various current distributions, which indicate the sensitivity of the reflector system to tilt angles of the reflector system with respect to the radome.

## REFERENCES


[1] K. S. Yee, "Numerical solution of initial boundary value problems involving Maxwell's equations in isotropic media," *IEEE Trans. Antennas Propagat.*, vol. AP-14, pp. 302–307, May 1966.

[2] W. Yu, D. Arakaki, and R. Mittra, "On the solution of a class of large body problems with full or partial circular symmetry by using the finite difference time domain (FDTD) method," *IEEE Trans. Antennas Propagat.*, vol. 49, pp. 1810–1817, Jan. 2001.

[3] Y. Chen and R. Mittra, "Finite-difference time-domain algorithm for solving Maxwell's equations in rotationally symmetric geometries," *IEEE Trans. Microwave Theory Tech.*, vol. 44, pp. 832–839, June 1996.

[4] G. Mur, "Absorbing boundary conditions for the finite-difference approximation of the time-domain electromagnetic field equations," *IEEE Trans. Electromagn. Compat.*, vol. EC-23, pp. 377–382, Mar. 1981.

[5] J. P. Berenger, "A perfectly matched layer for the absorption of electromagnetic waves," *J. Computat. Phys.*, vol. 114, pp. 185–200, 1994.

[6] R. Mittra, S. Dey, S. Chakravarty, and N. V. Veremey, "Reciprocity approach to pattern computation of a microstrip antenna operating in a complex environment," in *Proc. IEEE AP-S Int. Symp.*, Atlanta, GA, 1998, pp. 1138–1141.